Raman Spectral Analysis of Metal-Insulator Transitions in Skutterudite Compound $PrRu_4P_{12}$

N. Ogita,[1,*] R. Kojima,[1] T. Hasegawa,[1] H. Sugawra,[2] H. Sato,[3] and M. Udagawa[1,4]

[1] *Graduate School of Integrated Arts and Sciences, Hiroshima University, Higashi-Hiroshima, Japan*

[2] *Faculty of Integrated Arts and Sci., The University of Tokushima, Tokushima, Japan*

[3] *Department of Physics, Tokyo Metropolitan University, Tokyo, Japan*

[4] *Institute for Advanced Material Research, Hiroshima University, Higashi-Hiroshima, Japan*

(Received April 12, 2010)

Raman scattering spectra of $PrRu_4P_{12}$ have been measured to clarify the mechanism underlying the metal-insulator transition occurring in this compound at $T_{MI} = 63$ K. From the crystal electric field (CEF) excitation energies observed in the Raman spectra, the CEF level scheme is determined. A low-lying singlet-triplet CEF state is formed because of the competition between the field from the slightly transformed regular icosahedrons formed by the 12 P atoms and the cubic field from 8 coordination of Ru. The anomalous temperature dependence of the CEF excitation and phonon peak widths is strongly related to charge density wave (CDW) formation, which in turn is associated with the hybridization between the f and conduction electrons.

PACS numbers: 74.25.nd, 71.30.+h, 71.70.Ch

I. INTRODUCTION

Pr skutterudite compounds (PrT_4X_{12}; T: transition metal; X: pnictogen) have gained considerable importance because of their attractive properties. $PrFe_4P_{12}$, which is in the heavy-electron state, undergoes a phase transition to a nonmagnetic ordered state at 6.5 K [1]. This transition can be attributed to the antiferro-type ordering of the higher rank multipole in $PrFe_4P_{12}$ [2]. The metal-insulator transition in $PrRu_4P_{12}$ at $T_{MI} = 63$ K is accompanied by structural changes and is indicative of the formation of a new charge density wave (CDW), which is supported by the hybridization between the localized f electrons and the conduction electrons [3–5]. $PrOs_4Sb_{12}$, a heavy-electron superconductor, shows a field-induced ordered state; this can be explained on the basis of the induced moment in the antiferro-quadrupolar ordering [6, 7]. Extensive studies on skutterudite compounds have helped in gaining an in-depth understanding of the role of f electrons in the formation of the abovementioned ordered state.

Skutterudite compounds crystallize in a body-centered cubic structure and belong to the *Im-3* space group (point group *Th*), as shown in Fig. 1. The 12 X atoms at the 24g site $(0, u, v)$ form an icosahedral cage, and the Pr ion (2a site) is located at the center of the cage. The T atoms occupy the 8c$(1/4, 1/4, 1/4)$ sites, which are located between the

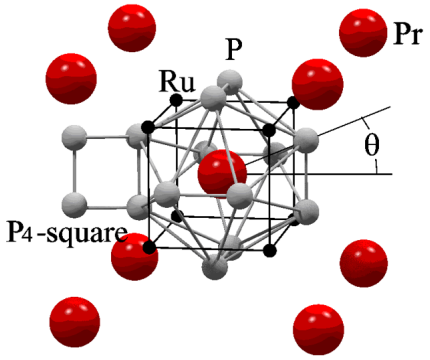

FIG. 1: Crystal structure of skutterudite compound $PrRu_4P_{12}$. The P and Ru ligands around the 8 Pr ions at the corner positions are not depicted. For more details, see text.

icosahedrons in the [111] direction [8].

The electronic properties and lattice dynamics of skutterudites result from the highly symmetrical cage structure of these compounds. When the cage size is large, the Pr ion is weakly bound to the cage and hence vibrates with a large amplitude. Consequently, the vibration is anharmonic. Anharmonicity of atomic vibrations is regarded as one of the most important characteristics of high-performance thermoelectric materials. Such anharmonic vibrations are occasionally given the name "rattling" [9]. On the other hand, the crystal electric field (CEF) splitting in skutterudites is small because of the highly symmetric configuration of the ligands. The CEF state $(4f^2, J = 4)$ of trivalent Pr ion has *Th* symmetry, and it splits into a singlet Γ_1 state, a doublet Γ_{23} state, and two triplet states ($\Gamma_4^{(1)}$ and $\Gamma_4^{(2)}$) [10].

The Γ_1 and Γ_{23} states in *Th* symmetry are identical to the Γ_1 and Γ_3 states in *Oh* symmetry, respectively. However, the $\Gamma_4^{(1)}$ and $\Gamma_4^{(2)}$ states are represented as mixtures of the Γ_4 and Γ_5 states with *Oh* symmetry. The ground and first excited CEF states for most Pr skutterudites are singlet-triplet states with a small energy splitting, such as Γ_1–$\Gamma_4^{(1)}$ or Γ_1–$\Gamma_4^{(2)}$. Such state with small energy splitting between the ground and excited CEF state is named as "quasi-quartet CEF ground state." Investigation of low-lying singlet-triplet CEF levels is important for understanding the numerous ordered states observed in the case of Pr skutterudites.

Therefore, in order to clarify the formation mechanism for the various ordered states in Pr skutterudites, it is important to investigate the behavior of the phonons and CEF states in these skutterudites at different temperatures, magnetic fields, etc. In this study, we measured the Raman scattering spectra of $PrRu_4P_{12}$ at various temperatures in order to understand the mechanism underlying the metal-insulator transition in this compound.

II. EXPERIMENT

Single crystals of $PrRu_4P_{12}$ were synthesized by the Sn flux method. Raman scattering spectra were measured by using the multichannel detection systems. An Ar ion laser operated at 488.0 nm or 514.5 nm was employed the excitation source (output power: 5 mW). The scattered light was dispersed by a triple monochromator (JASCO model U–1800) and analyzed by a liquid-nitrogen-cooled CCD detector (Princeton Instruments Inc., Model LN/CCD–1100–PB).

Because $PrRu_4P_{12}$ belongs to the *Im-3* space group, the Raman-active modes appear at the center of the Brillouin zone; $\Gamma = 2A_g + 2E_g + 4T_g$, as per Mulliken's notation. A_g, E_g, and T_g are singlet, doublet, and triplet irreducible representations corresponding to the Bethe notations Γ_1, Γ_{23}, and $\Gamma_4^{(1)}$ ($\Gamma_4^{(2)}$), respectively. Since $PrRu_4P_{12}$ has cubic symmetry, the A_g (or Γ_1) and T_g modes are observed in the spectra recorded in the (x, x) and (x, y) polarization geometries, respectively, while the E_g mode is observed in the spectra recorded in the $(x+y, x-y)$ and (x, x) polarization geometries. All the Raman-active modes appear in the spectrum recorded in the $(x+y, x+y)$ polarization geometry. In the notation (x, y), x and y denote the direction of polarization of the incident and scattered light, respectively. x and y also correspond to the [100] and [010] crystal axes, respectively. In this paper, we use the Mulliken and Bethe notations for the phonons and CEF states, respectively. In the case of the phonons, the Raman-active modes $2A_g + 2E_g + 4T_g$ are due to the vibrations of the pnicogen atoms.

III. DISCUSSION

Figure 2 shows the temperature dependence of the Raman scattering spectra recorded in $(x-y, x+y)$ polarization geometry. Each spectrum is shifted along the logarithmic scale to avoid crossing of the spectrum. The arrows at the center of the longitudinal axes indicate the metal-insulator transition temperature T_{MI} (63 K).

In the spectrum recorded at temperatures above T_{MI}, two peaks corresponding to the $2E_g$ phonon modes appear at around 360 and 430 cm^{-1}. The former and latter peaks correspond to the stretching and bending vibrations of the Pr–P bonds, respectively. The energies of these vibrations are mainly dominated by the rigid P–P bonds in the P_4 square (see Fig. 1). The width of the Pr–P stretching peak is greater than that of the Pr–P bending peak, suggesting that large-amplitude vibrations of the Pr ions affect the motion of the P ligands, although the Pr–P bonds in this skutterudite are weak. On the other hand, the broad peaks in the low-energy region of the spectrum (below 200 cm^{-1}) are assigned to the Pr ion vibrations caused by second-order Raman scattering (open triangle) and CEF excitation (closed triangles). These assignments are consistent with the phonon dispersion relations determined by X-ray and neutron inelastic scattering experiments [11, 12] and those derived from first-principle calculations. The assignment of the CEF excitation peaks is also consistent with the results of neutron scattering [13] and the observed asymmetric Raman components, that is, the results of comparison of the Raman spectra recorded in

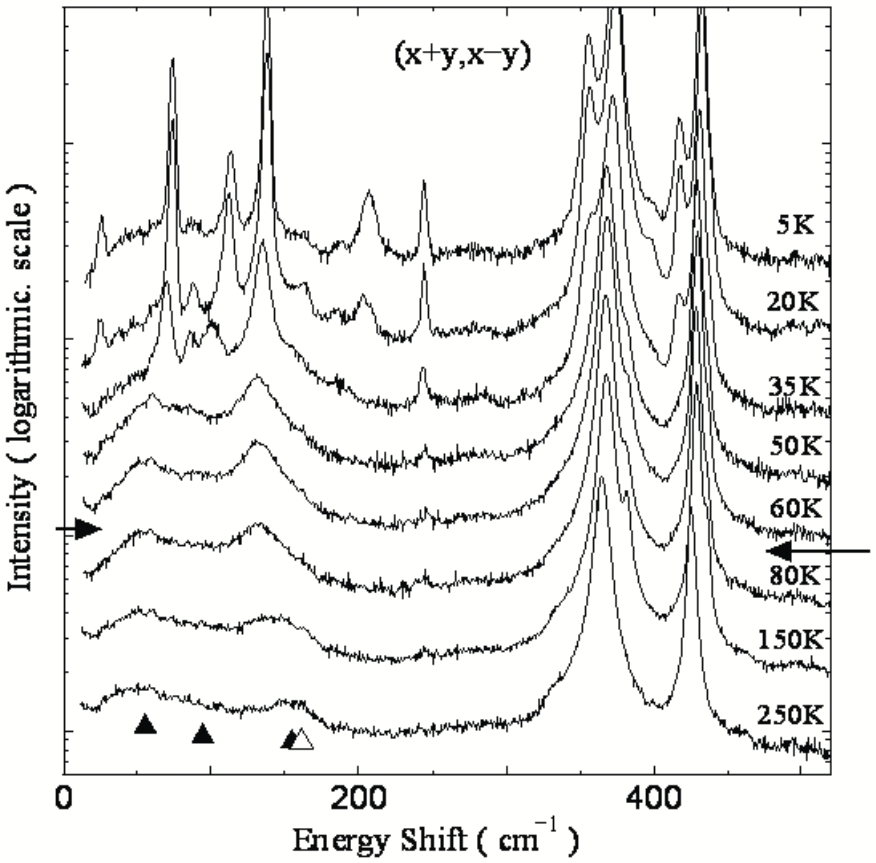

FIG. 2: Temperature dependence of Raman spectra of $PrRu_4P_{12}$. For details, see text.

the (x, y) and (y, x) polarization geometries. The main CEF excitation peaks in the spectra are due to $\Gamma_4^{(1)}$–$\Gamma_4^{(2)}$, Γ_1–$\Gamma_4^{(2)}$, and Γ_1–Γ_{23} transitions.

When the temperature is decreased below T_{MI}, the spectrum shows several peaks that can be attributed to the structural changes occurring in $PrRu_4P_{12}$. At T_{MI}, the crystallographic symmetry changes from space group *Im-3* to *Pm-3* [14], corresponding to a cell-doubling transition; this is because the Ru and P ligands are displaced, and hence, the equivalent Pr ions at the center and 8 corners of the cubic unit (shown in Fig. 1) become non-equivalent. As a result, peaks due to zone-folded phonons are expected to appear in the spectrum. The new peaks in the high-energy region can be assigned to the zone-folded phonons corresponding to P atom vibrations. All the new peaks in the low-energy region can be assigned to CEF excitations, except for the strong peak at around 140 cm^{-1}; this peak is due to the accidental overlap between the CEF excitation peak and the zone-folded phonon peak. Because of the presence of two inequivalent Pr ions, two CEF excitation peaks are observed, one attributable to Pr1 (located at the center of the cubic unit as

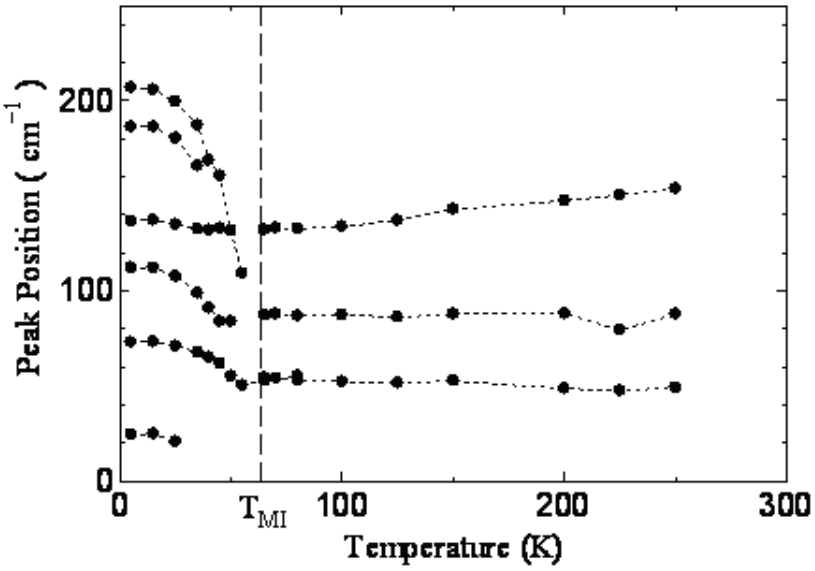

FIG. 3: Temperature dependence of CEF energy observed in $(x + y, x - y)$ spectra.

shown in Fig. 1) and the other attributable to Pr2 (located at 8 corners of the cubic unit). Hereafter, we focus only on the CEF excitation peak observed in the Raman spectra.

The temperature dependence of the CEF excitation energy is shown in Fig. 3. As shown in the figure, the CEF excitation peaks are clustered with a decrease in temperature, and at T_{MI}, the peaks split. Below T_{MI}, the energy of each peak changes drastically until T falls to approximately 20 K.

Figure 4 shows the polarization dependence determined at T = 4.6 K in the CEF energy region. The spectra show the assignment of the CEF excitation peaks for Pr1 and Pr2. In a previous study [13], the CEF energy levels determined at 5 K by neutron inelastic scattering experiments were Γ_1–$\Gamma_4^{(2)}$ (8.14 meV)–$\Gamma_4^{(1)}$ (9.27 meV)–Γ_{23} (15.86 meV) for Pr1 and $\Gamma_4^{(2)}$–Γ_1 (3.12 meV)–$\Gamma_4^{(1)}$ (13.88 meV)–Γ_{23} (20.05 meV) for Pr2. The highest-energy transition is the $\Gamma_4^{(2)}$–Γ_{23} (20.05 meV) transition in Pr2. The peak due to this transition is not observed in neutron scattering experiments [13] because of the small magnetic moment associated; however, this peak appears at 210 cm^{-1} in the Raman spectra, as shown in Fig. 4. Therefore, there might be a change in the $\Gamma_4^{(2)}$–χ transition energy, which is the highest among all the transition energies considered in this study. From the energies of the CEF peaks observed in the Raman spectra, we analyzed the CEF energy schemes by employing the CEF Hamiltonian for the $4f$ electrons in Th symmetry:

$$\mathcal{H}_{\rm CEF} = A_4(O_4^0 + 5O_4^4) + A_6(O_6^0 + 5O_6^4) + A_6^{\rm T}(O_6^2 + 5O_6^6), \tag{1}$$

where $O_{\rm m}^{\rm n}$ represents the Stevens operator equivalent. The third term in the abovementioned equation is attributed to the absence of C_4 point symmetry when the Pr site is in

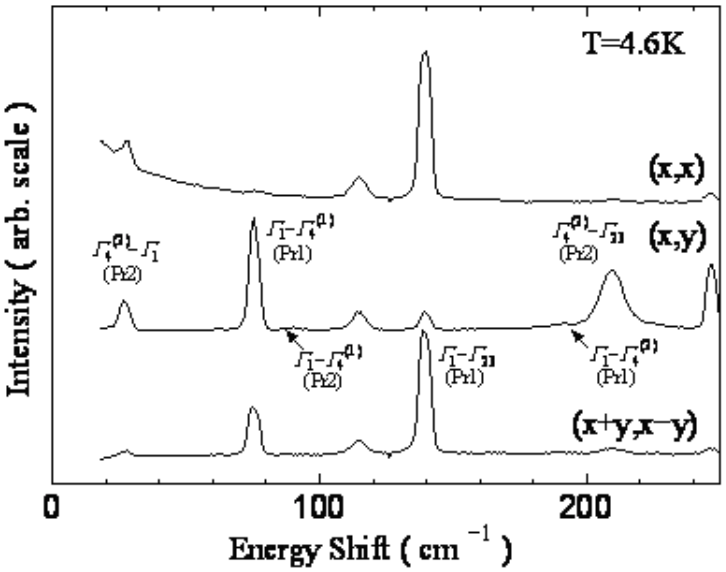

FIG. 4: Polarization dependence of Raman spectra of $PrRu_4P_{12}$ at 4.6 K.

Th symmetry [10]. Thus, we derive the following energy schemes at T = 4.6 K: Γ_1–$\Gamma_4^{(1)}$ (9.3 meV)–Γ_{23} (17.4 meV)–$\Gamma_4^{(2)}$ (23.7 meV) for Pr1 and $\Gamma_4^{(2)}$–Γ_1 (3 meV)–$\Gamma_4^{(1)}$ (16 meV)–Γ_{23} (25.3 meV) for Pr2. In this calculation, we assume the parameter A_6^{T} for Pr2 to be zero. The obtained result is not accurate because the local symmetry of Pr2 does not change. Therefore, further investigation is necessary for a quantitative estimation of the CEF energy. However, the present results can be used for a qualitative discussion, that is, for proposing the CEF level scheme. The CEF level scheme determined for Pr1 by neutron scattering experiments (Γ_1–$\Gamma_4^{(2)}$–$\Gamma_4^{(1)}$–Γ_{23}) is different from that determined by Raman spectral measurements in the present study (Γ_1–$\Gamma_4^{(1)}$–Γ_{23}–$\Gamma_4^{(2)}$).

As shown in Fig. 1, the presence of P and Ru ligands causes the local symmetry of the Pr ion to become *Th* and *Oh*, respectively. Therefore, we rewrite the CEF Hamiltonian as

$$\mathcal{H}_{\mathrm{CEF}} = (1-x)\mathcal{H}_{\mathrm{CEF}}^{\mathrm{P}}(\theta) + x\,\mathcal{H}_{\mathrm{CEF}}^{\mathrm{Ru}}, \tag{2}$$

where θ corresponds to the pnictogen position ($\theta = \tan^{-1}(v/u)$), shown in Fig. 1. In case of $PrRu_4P_{12}$, θ is 21.8° at room temperature. When $\theta = 31.7°$ and $x = 0$, the icosahedral configuration has *Ih* symmetry, which is a "regular icosahedral." In this symmetry, the CEF scheme of Pr ion is a *Hg* (Γ_4) quintet and a *Gg* (Γ_5) quartet CEF state. When the P ligands carry a negative charge, the *Hg* state becomes the CEF ground state. With θ is decreased to 21.8°, *Hg* splits into $\Gamma_4^{(1)}$ and Γ_{23}, while *Gg* splits into Γ_1 and $\Gamma_4^{(2)}$. Figure 5(a) shows the dependence of the CEF level scheme on θ, only for the P ligands ($x = 0$). As shown in the figure, the CEF level scheme at $\theta = 21.8°$ is Γ_1–$\Gamma_4^{(1)}$–Γ_{23}–$\Gamma_4^{(2)}$, which is the

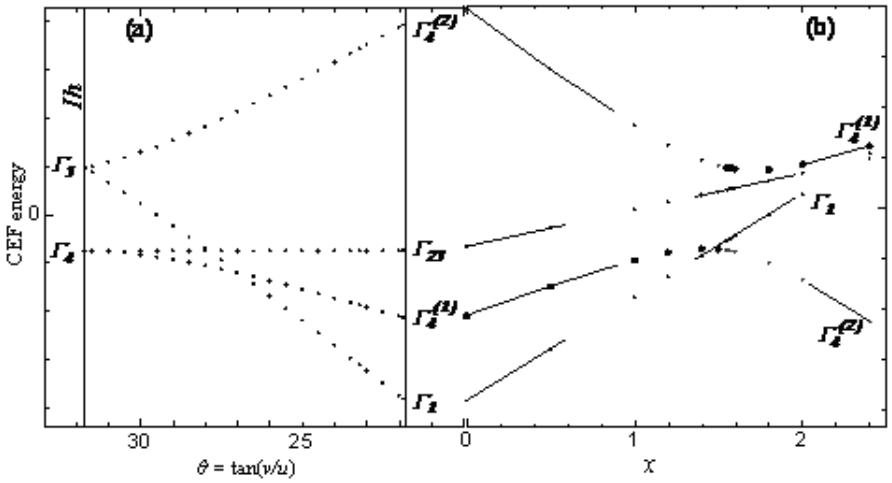

FIG. 5: CEF level scheme for $PrRu_4P_{12}$ as a function of x and θ in Eq. (2).

same as the CEF level scheme for Pr1 at temperatures below T_{MI}.

Figure 5(b) shows the CEF level scheme as a function of x in Eq. (2). With an increase in x, the CEF effect caused by the Ru ligands becomes stronger. As shown in the figure, with an increase in x to approximately 1.4, the energies of the CEF states become similar. This may compensate for the CEF effect of the P ligands [10, 15]. The ground state changes from Γ_1 to $\Gamma_4^{(1)}$ when $x \sim 1.4$. At $x \sim 1.5$, the triplet states $\Gamma_4^{(1)}$ and $\Gamma_4^{(2)}$ are interchanged, although there is no mixing of these two states. As a consequence, the $\Gamma_4^{(2)}$ ground state (as determined by Raman and neutron scattering experiments) of Pr2 is reproduced in the region above $x(\mathrm{Pr2}) = 1.5$. On the other hand, because the CEF level scheme of Pr1 is Γ_1–$\Gamma_4^{(1)}$–Γ_{23}–$\Gamma_4^{(2)}$, x(Pr1) is in the region of $x \sim 1$–2. The value of x for the CEF state at temperatures above T_{MI} appears to be between x(Pr1) and x(Pr2). Therefore, metal-insulator transition is caused by the CEF compensation between P and Ru ligands or by the case of low-lying CEF states. These discussions are based on the point-charge model. In reality, the charge distribution is very complex, and the Hamiltonian cannot be directly split in the manner shown in Eq. (2). Hence, we restrict ourselves to a qualitative discussion of the CEF level scheme.

According to a theoretical study, the metal-insulator transition can be attributed to the antiferro order of hexadecapole moments with Γ_{1g} symmetry [16]. On the other hand, another study states that this transition is due to CDW formation, which can be attributed to the quasi-quartet CEF state and the hybridization between the f and conduction electrons. At T_{MI}, there is a difference in the charge distribution in the icosahedrons because of the presence of P atoms around Pr1 and Pr2 [17]. When the temperature ranges from 20 K to just below T_{MI}, a hump corresponding to CDW formation is observed in the temperature dependence of the electronic resistance [3]. As shown in Fig. 2, the CEF excitation peaks are broad at around T_{MI}, and the peak widths rapidly decrease when T is approximately

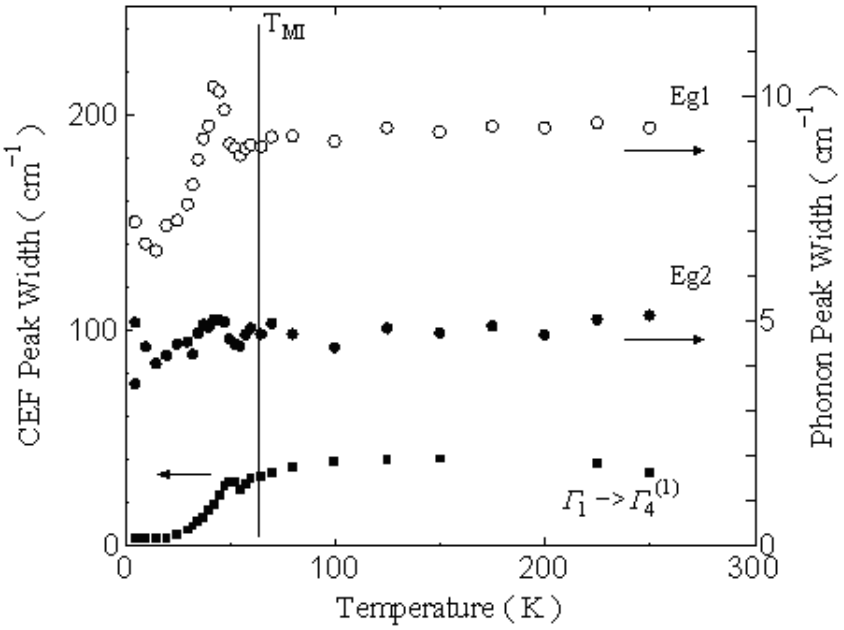

FIG. 6: Temperature dependence of CEF and phonons peak widths for of $PrRu_4P_{12}$. For details, see text.

20 K. Figure 6 shows the temperature dependence of the peak width for the representative CEF excitation and phonon peaks. As shown in the figure, the peak width begins to decrease at temperatures slightly above T_{MI}. No notable anomaly is observed at T_{MI}. This broadening of the CEF excitation peak is probably due to the hybridization between the f and conduction electrons [18]. In the case of $PrOs_4P_{12}$, the broadening of the CEF peak is well explained on the basis of the aforementioned hybridization [19]. On the other hand, the width of the E_{g1} phonon peak, which is attributed to the stretching vibrations of the Pr–P bond, shows an anomaly in the temperature range in which CDW formation is observed. Therefore, this anomaly is indicative of electron-phonon coupling during CDW formation.

Quantitative analysis of the CEF schemes has not been successfully carried out. Nevertheless, the results of the present study indicate that the anomalous behavior of the widths of the CEF excitation and phonon peaks is closely related to CDW formation, which in turn is associated with the hybridization between the f and conduction electrons.

IV. CONCLUSIONS

Raman scattering spectra of $PrRu_4P_{12}$ have been measured to elucidate the mechanism underlying the metal-insulator transition observed at $T_{MI} = 63$ K in this compound. The CEF level scheme for this compound is determined from the CEF excitation energies

observed in the Raman spectra. From a simple discussion based on the point-charge model, it is proposed that a low-lying singlet-triplet CEF state is formed by the competition between the slightly transformed icosahedrons of P and the cubic field of Ru. The anomalous temperature dependence of the CEF excitation peak widths is indicative of hybridization between the f and conduction electrons. The change in the phonon peak width is related to the electron-phonon coupling during CDW formation.

Acknowledgments

We thank Professor H. Shiba and K. Iwasa for valuable discussions. This study was supported by a Grant-in-Aid for Scientific Research on Innovative Areas "Heavy Electrons" (No. 20102005) of The Ministry of Education, Culture, Sports, Science, and Technology, Japan, and by N-BARD and IAMR of Hiroshima University.

References

* Electronic address: nogita@hiroshima-u.ac.jp

[1] Y. Aoki *et al.*, Phys. Rev. B **65**, 064446 (2002).
[2] A. Kiss and Y. Kuramoto, J. Phys. Soc. Jpn. **75**, 103704 (2006).
[3] C. Sekine *et al.*, Phys. Rev. Lett. **79**, 3218 (1997).
[4] H. Harima and K. Takegahara, Physica B **312–313**, 843 (2002).
[5] S. R. Shaha *et al.*, Phys. Rev. B **71**, 132502 (2005).
[6] Y. Aoki *et al.*, J. Phys. Soc. Jpn. **71**, 2098 (2002).
[7] T. Tayama *et al.*, J. Phys. Soc. Jpn. **72**, 1516 (2003).
[8] Sales, *Handbook on the Physics and Chemistry of Rare Earths*, vol. 33 (Amsterdam: Elsevier Science BV) p1.
[9] T. Goto *et al.*, Phys. Rev. B **69**,180511(R) (2004).
[10] K. Takegahara, H. Harima and A. Yanase, J. Phys. Soc. Jpn. **70**, 1190 (2001); **70**, 3468 (2001).
[11] S. Tsutsui *et al.*, J. Phys. Soc. Jpn. **77**, 033601 (2008).
[12] C. H. Lee *et al.*, J. Phys. Soc. Jpn. **75**, 123602 (2006).
[13] K. Iwasa *et al.*, Phys. Rev. B **72**, 024414 (2005); J. Phys. Soc. Jpn. **74**, 1930 (2005).
[14] C. H. Lee *et al.*, Phys. Rev. B **70**, 153105 (2004).
[15] J. Otsuki *et al.*, J. Phys. Soc. Jpn. **74**, 200 (2005).
[16] T. Takimoto, J. Phys. Soc. Jpn. **75**, 034714 (2006).
[17] R. Shiina and R. Shiina, J. Phys. Soc. Jpn. **77**, 083705 (2008); **78**, 104722 (2009); **79**, 044704 (2010).
[18] K. W. Becker, P. Flude and J. Keller, Z. Physik B **28**, 9 (1977).
[19] K. Iwasa *et al.*, Phys. Rev. B **79**, 235113 (2009).